Precise measurements of the $K_S \to \gamma\gamma$ and $K_L \to \gamma\gamma$ decay rates

NA48 collaboration

A. Lai, D. Marras

Dipartimento di Fisica dell'Università e Sezione dell'INFN di Cagliari, I-09100 Cagliari, Italy

J.R. Batley, R.S. Dosanjh, T.J. Gershon, G.E. Kalmus, C. Lazzeroni, D.J. Munday, E. Olaiya, M.A. Parker, T.O. White, S.A. Wotton

Cavendish Laboratory, University of Cambridge, Cambridge, CB3 0HE, U.K.[1]

R. Arcidiacono[2], G. Barr, G. Bocquet, A. Ceccucci, T. Cuhadar-Dönszelmann, D. Cundy[3], N. Doble, V. Falaleev, L. Gatignon, A. Gonidec, B. Gorini, P. Grafström, W. Kubischta, A. Lacourt, I. Mikulec[4], A. Norton, B. Panzer-Steindel, G. Tatishvili[5], H. Wahl

CERN, CH-1211 Genève 23, Switzerland

C. Cheshkov, P. Hristov, V. Kekelidze, D. Madigojine, N. Molokanova, Yu. Potrebenikov, A. Zinchenko

Joint Institute for Nuclear Research, Dubna, Russian Federation

V. Martin, P. Rubin, R. Sacco, A. Walker

Department of Physics and Astronomy, University of Edinburgh, JCMB King's Buildings, Mayfield Road, Edinburgh, EH9 3JZ, U.K.

M. Contalbrigo, P. Dalpiaz, J. Duclos, P.L. Frabetti, A. Gianoli, M. Martini, F. Petrucci, M. Savrié

Dipartimento di Fisica dell'Università e Sezione dell'INFN di Ferrara, I-44100 Ferrara, Italy

A. Bizzeti[6], M. Calvetti, G. Collazuol, G. Graziani, E. Iacopini, M. Lenti, F. Martelli, M. Veltri

Dipartimento di Fisica dell'Università e Sezione dell'INFN di Firenze, I-50125 Firenze, Italy

M. Eppard, A. Hirstius, K. Holtz, K. Kleinknecht, U. Koch, L. Köpke, P. Lopes da Silva, P. Marouelli, I. Mestvirishvili, I. Pellmann, A. Peters, S.A. Schmidt, V. Schönharting, Y. Schué, R. Wanke, A. Winhart, M. Wittgen

Institut für Physik, Universität Mainz, D-55099 Mainz, Germany[7]

J.C. Chollet, L. Fayard, L. Iconomidou-Fayard, G. Unal, I. Wingerter-Seez

Laboratoire de l'Accélérateur Linéaire, IN2P3-CNRS,Université de Paris-Sud, 91898 Orsay, France[8]

G. Anzivino, P. Cenci, E. Imbergamo, P. Lubrano, A. Mestvirishvili, A. Nappi, M. Pepe, M. Piccini

Dipartimento di Fisica dell'Università e Sezione dell'INFN di Perugia, I-06100 Perugia, Italy

R. Casali, C. Cerri, M. Cirilli[9], F. Costantini, R. Fantechi, L. Fiorini, S. Giudici,

I. Mannelli, G. Pierazzini, M. Sozzi

Dipartimento di Fisica, Scuola Normale Superiore e Sezione dell'INFN di Pisa, I-56100 Pisa, Italy

J.B. Cheze, M. De Beer, P. Debu, F. Derue, A. Formica, R. Granier de Cassagnac, G. Gouge, G. Marel, E. Mazzucato, B. Peyaud, R. Turlay, B. Vallage

DSM/DAPNIA - CEA Saclay, F-91191 Gif-sur-Yvette, France

M. Holder, A. Maier, M. Ziolkowski

Fachbereich Physik, Universität Siegen, D-57068 Siegen, Germany[10]

C. Biino, N. Cartiglia, F. Marchetto, E. Menichetti, N. Pastrone

Dipartimento di Fisica Sperimentale dell'Università e Sezione dell'INFN di Torino, I-10125 Torino, Italy

J. Nassalski, E. Rondio, M. Szleper, W. Wislicki, S. Wronka

Soltan Institute for Nuclear Studies, Laboratory for High Energy Physics, PL-00-681 Warsaw, Poland[11]

H. Dibon, M. Jeitler, M. Markytan, G. Neuhofer, M. Pernicka, A. Taurok, L. Widhalm

Österreichische Akademie der Wissenschaften, Institut für Hochenergiephysik, A-1050 Wien, Austria[12]

Abstract

The $K_S \to \gamma\gamma$ decay rate has been measured with the NA48 detector using a high intensity short neutral beam from the CERN SPS. The measured branching ratio $BR(K_S \to \gamma\gamma) = (2.78 \pm 0.06_{stat} \pm 0.04_{syst}) \times 10^{-6}$, obtained from 7461 ± 172 $K_S \to \gamma\gamma$ events, is significantly higher than the $O(p^4)$ prediction of Chiral Perturbation Theory. Using a K_L beam the ratio $\frac{\Gamma(K_L \to \gamma\gamma)}{\Gamma(K_L \to \pi^0\pi^0\pi^0)} = (2.81 \pm 0.01_{stat} \pm 0.02_{syst}) \times 10^{-3}$ has been measured.

1   Introduction

The decays $K_{S,L} \to \gamma\gamma$ and $K_{S,L} \to \pi^0\gamma\gamma$ are important probes of Chiral Perturbation Theory (χPT), an effective field theory of the Standard Model at low energies. The decay amplitude of $K_S \to \gamma\gamma$ can be calculated unambiguously at the leading $O(p^4)$ order of the perturbative expansion giving a branching ratio of 2.1×10^{-6} with an uncertainty of only a few per cent [1][1]. The theoretical predictions for $K_L \to \gamma\gamma$ are much less accurate [3]. The $K_S \to \gamma\gamma$ decay rate has hitherto been considered as an example of good agreement between the χPT prediction and the experimental measurement $(2.4\pm0.9)\times10^{-6}$, obtained by the NA31 experiment [4]. This result was recently improved by NA48 to $(2.58 \pm 0.42) \times 10^{-6}$ [5] with data from a two-day test run with high intensity short neutral beam, collected in September 1999. However, the previous experimental results are not precise enough to resolve the higher order effects which are predicted by the χPT to be at most of the order of $m_K^2/(4\pi F_\pi)^2 \sim 20\%$ of the $O(p^4)$ decay amplitude [1]. Using data taken in a 40 day run with the high intensity short neutral beam in the year 2000, for the first time an accuracy of a few % has been achieved. A comparison of the experimental result with the $O(p^4)$ χPT prediction allows the estimation of the $O(p^6)$ loop contributions. According to χPT, these could also contribute to $O(p^6)$ effects in the $K_L \to \pi^0\gamma\gamma$ decay which up to now are believed to be dominated by vector meson exchange.

2   Principle of the measurement

The NA48 experiment has been designed to measure direct CP violation in neutral kaon decays and comprises K_S and K_L beams created at two targets, near and far from the decay region, which can be run together or separately [6].

In previous measurements of $K_S \to \gamma\gamma$, the decay region used contained almost twice as many decays coming from $K_L \to \gamma\gamma$. Their subtraction using the K_L flux estimated from e.g. $K_L \to \pi^0\pi^0\pi^0$ decays introduces an uncertainty of more than 4% due to the poorly known $K_L \to \gamma\gamma$ branching ratio. In the measurement presented here, this problem is overcome by using a novel method based on the observed ratio of $K_L \to \gamma\gamma$ to $K_L \to \pi^0\pi^0\pi^0$, as a function of energy and decay position, in the K_L beam (far-target) run performed immediately prior to the K_S beam (near-target) data taking. As the near- and far-target beams are almost collinear and have similar momentum spectra, the measurement of $K_L \to \pi^0\pi^0\pi^0$ decays in the near-target beam, as a function of energy and decay position, and the ratio $N^{far}_{K_L \to \gamma\gamma}/N^{far}_{K_L \to \pi^0\pi^0\pi^0}$ measured from the far-target beam allow the direct evaluation of the number of $K_L \to \gamma\gamma$ decays in the near-target beam. By using the same ranges of energy and decay position only a very small acceptance correction is needed due to the slight differences in geometries of the two beams. A by-product of this method is a precise measurement of $\frac{\Gamma(K_L \to \gamma\gamma)}{\Gamma(K_L \to \pi^0\pi^0\pi^0)}$.

3   Experimental set-up and data taking

The near-target beam contains K^0 mesons and hyperons. It was produced on a 2 mm diameter, 400 mm long beryllium target by 400 GeV protons at a production angle of 3.0 mrad in the vertical plane. In this special high intensity near-target mode, the primary proton beam was attenuated and collimated to the desired intensity, far upstream of the target. The target is followed by a sweeping magnet packed with tungsten-alloy inserts in which protons not interacting in the target are absorbed, and by a 0.36

---

[1] These results are similar to those obtained in earlier calculations based on a phenomenological approach [2]

cm diameter collimator. In the usual NA48 experimental configuration the 1.5 m long collimator is followed successively by an anti counter (AKS), by an 89 m long evacuated tube terminated by a thin Kevlar window and by a helium filled tank which contains the drift chambers and a spectrometer magnet. However for these data the AKS counter, the Kevlar window and the drift chambers were removed and the helium tank was evacuated.

The present analysis is based on data recorded during a 40-day run in 2000 with a beam intensity of about $\sim 10^{10}$ protons hitting the target during the 3.2 s long SPS spill. This is a factor of ~ 300 higher than the usual near-target beam. This near-target run was preceded by a 30-day run with the far-target beam alone and the same detector configuration[2], devoted mainly to studies of systematic effects in the direct CP-violation measurement [7, 8].

The detector elements used in the analysis are the following:

– A liquid krypton calorimeter (LKr) [9] is used to measure the energy, position and time of electro-magnetic showers initiated by photons (γ). Around 20 t of liquid krypton at 121 K are used as an ionization detector. The calorimeter has a structure of 13212 square towers of 2×2 cm^2 cross-section and 127 cm length (27 radiation lengths) each. The cells are formed by copper-beryllium ribbons, 1.8 cm wide and 40 μm thick, stretched longitudinally. The ionization signal from each of the cells is amplified, shaped, and digitised by 10-bit FADCs at 40 MHz sampling frequency. The dynamic range of the digitisers is increased by gain-switching amplifiers which change the amplification factor depending on the pulse height. The energy resolution is

$$\sigma(E)/E \simeq 0.090/E \oplus 0.032/\sqrt{E} \oplus 0.0042, \qquad (1)$$

where E is in GeV. The read-out system was calibrated by a charge pulse every burst during data taking. The final calibration of the energy scale is fixed by fitting the effective edge of the collimator seen in the data to be the same as in the Monte Carlo. The relative calibrations of the individual cells were determined by using K_{e3} decays during the 1998 run and checked to be similar in the 2000 run with $\pi^0, \eta \to \gamma\gamma$ decays produced in thin targets in a special π^--beam run. The position and time resolutions for a single photon with energy larger than 20 GeV are better than 1.3 mm and 300 ps, respectively.

– A sampling hadron calorimeter composed of 48 steel plates, each 24 mm thick, interleaved with scintillator planes is used to measure hadronic showers with a readout in horizontal and vertical projections.

– A scintillator hodoscope upstream of the two calorimeters helps to detect charged particles. It is composed of two planes segmented in horizontal and vertical strips arranged in four quadrants.

A more complete description of the apparatus can be found elsewhere [8].

The trigger decision, common to $\gamma\gamma$, $\pi^0\pi^0$ and $\pi^0\pi^0\pi^0$ decays, is based on quantities which are derived from the projections of the energy deposited in the electro-magnetic liquid krypton calorimeter [10]. The trigger required that the total deposited energy E_{tot} is larger than 50 GeV, the radius of the centre of energy is smaller than 15 cm and the proper life time of the kaon is less than 9 K_S lifetimes downstream of the collimator. The trigger efficiency, $(99.8 \pm 0.1)\%$, is measured using a minimum-bias sample triggered by a

---

[2] with exception of the proton beam energy which was 450 GeV, production angle which was 4.2 mrad and of the spectrometer magnet which, unlike in the near-target run, was powered in order to create occupancy conditions as close as possible to those of the direct CP-violation measurement.

2

scintillating fibre hodoscope placed in the liquid krypton calorimeter and is equal for $\gamma\gamma$, $\pi^0\pi^0$ and $\pi^0\pi^0\pi^0$ decays in both the near- and far-target runs.

4   Event selection

The energies and positions of electro-magnetic showers initiated by photons, measured in the liquid krypton calorimeter, are used to calculate the kaon energy and decay vertex. To select $K \rightarrow \gamma\gamma$ candidates, all events with ≥ 2 energy clusters are considered. Pairs of clusters which are in time within 5 ns and with no other cluster with energy > 1.5 GeV closer in time than 3 ns with respect to the event time are selected. The event time is computed from the times of the two most energetic cells of the selected clusters. In addition, the $\gamma\gamma$ pair must pass the following cuts:
  – The energy of each cluster must be greater than 3 GeV and less than 100 GeV.
  – The transverse distance between two clusters is required to be greater than 10 cm.
  – The total energy of the selected cluster pair is required to be less than 170 GeV and to be greater than 70 GeV.
  – The radius of the centre of energy,

$$R_C = \frac{\sqrt{(\sum_i E_i x_i)^2 + (\sum_i E_i y_i)^2}}{\sum_i E_i} \tag{2}$$

  is required to be less than 7 cm, where E_i, x_i, y_i are the $i-th$ cluster energy, x and y coordinates at LKr, respectively.
  – The energy deposited in the hadron calorimeter must not exceed 3 GeV in a time window of ± 15 ns around the event time.

In order to determine the K_S and K_L fluxes in the beam, the decays $K_S \rightarrow \pi^0\pi^0$ and $K_L \rightarrow \pi^0\pi^0\pi^0$ have been used. Similar conditions as for $\gamma\gamma$ cluster pairs are applied to groups of 4 or 6 in-time clusters for $2\pi^0$ and $3\pi^0$ respectively.

The decay vertex position z_{vertex} of a kaon decaying into photons or π^0's is calculated using the kaon mass constraint

$$z_{vertex} = z_{Lkr} - \frac{\sqrt{\sum_{i,j,i>j} E_i E_j[(x_i - x_j)^2 + (y_i - y_j)^2]}}{m_K} \tag{3}$$

where z_{Lkr} is the z coordinate of the LKr calorimeter with respect to the end of the collimator.

In $2\pi^0$ and $3\pi^0$ samples a χ^2 cut of 27 ($\sim 5\sigma$) is applied to the invariant masses of photon pairs calculated using z_{vertex}. For $2\pi^0$ decay, the χ^2 variable is defined as

$$\chi^2 = \left[\frac{(m_1 + m_2)/2 - m_{\pi^0}}{\sigma_+}\right]^2 + \left[\frac{(m_1 - m_2)/2}{\sigma_-}\right]^2 \tag{4}$$

where $\sigma_\pm$ are the resolutions on $(m_1 \pm m_2)/2$ measured from the data and parametrised as a function of the lowest photon energy. For $\pi^0\pi^0\pi^0$ decays an equivalent variable is defined in the space of three invariant masses.

Due to the large background from $K_S \rightarrow \pi^0\pi^0$ decays the study of $K_S \rightarrow \gamma\gamma$ can only be carried out in a restricted decay region. The maximum $\gamma\gamma$ mass from a $K_S \rightarrow \pi^0\pi^0$ decay where two photons escape detection is 458 MeV/c^2 which would lead to an apparent vertex shift of 9 m downstream. However, in case some showers overlap and only one or

no photon misses the detector this shift can be significantly smaller. Therefore the decay region is defined to be between -1 m and 5 m with respect to the exit of the collimator.

In order to remove events with hadronic or overlapping showers from the $\gamma\gamma$ sample, the shower width is required to be less than 3σ above the average value for photon showers of a given energy. This cut, which is calibrated from showers in $K_S \to \pi^0\pi^0$ decays, removes $< 0.5\%$ of good $K \to \gamma\gamma$ events.

In the near-target data, 19819 events passed the $\gamma\gamma$ selection cuts while in the far-target data more than 6×10^4 events were used. Normalisation channels were down-scaled, retaining several hundred thousand events for analysis.

5   Background subtraction

The $\pi^0\pi^0$ and $\pi^0\pi^0\pi^0$ samples are essentially background free. In the $\gamma\gamma$ samples the following backgrounds have been identified and subtracted:

– A small hadronic background visible as a tail in the shower width distribution. In the near-target sample this background originates from interactions of the beam particles in the collimator. In the far-target beam, which is cleaned by three collimators, the background from this source is negligible. However, pairs of charged hadrons generated in the far-target beam upstream of or inside the final collimator and opened vertically by the last sweeping magnet have been found to contribute to the $K_L \to \gamma\gamma$ sample.

– Accidental $\gamma\gamma$ pairs visible as a flat continuum in the distribution of the shower time differences.

– Residual $K_S \to \pi^0\pi^0$ decays with one shower overlap and one low-energy photon missing the calorimeter.

– Dalitz decay $K^0 \to ee\gamma$ with an overlapping ee pair or one shower with energy below the detection limit of 1.5 GeV. In the far-target run, due to the presence of magnetic field, ee pairs do not overlap.

The last three background sources contribute significantly only to the near-target $\gamma\gamma$ sample.

The hadronic and accidental backgrounds are subtracted using the distribution in radius of the centre of energy (R_C), which indicates the deviation of the direction of the apparent decay source from the beam axis. A control region is defined with R_C between 8 cm and 10 cm. In order to obtain the background-extrapolation factor to the signal region, $R_C < 7$ cm, a set of model distributions has been extracted from the data by modifying certain selection requirements.

In the near-target data, in order to study the hadronic background component two different samples have been selected. In one, a hit in the hadron calorimeter is required and the shower width cut is released (extrapolation factor 1.5). In the other sample, as collimator scattering can produce more than two particles, an additional shower in the calorimeter is required and the decay region is shortened by 1 m in order to avoid contamination from $K_S \to \pi^0\pi^0$ decays, while all other cuts are unchanged (extrapolation factor 3.1) (Fig. 1 left). The model of accidental background is obtained by requiring the two showers to be out of time by more than 5 ns and less than 10 ns (extrapolation factor 2.7). The median value of the extrapolation factors from three different models gives an inclusive hadronic and accidental background estimate of $(2.1 \pm 0.7)\%$ of the $K_S \to \gamma\gamma$ sample where the uncertainty corresponds to the spread of the extrapolation factors (Fig. 1 right).

4

In the far-target data the background model sample is obtained by requiring a hit in the hadron calorimeter and a hit in the scintillator hodoscope giving an extrapolation factor of 2.3. Using this factor and a conservative uncertainty leads to a background estimate of $(0.6 \pm 0.3)\%$ (Fig. 2). In both background estimates the amount of beam halo in the control region is taken into account and is estimated from $\pi^0\pi^0$ and $\pi^0\pi^0\pi^0$ samples.
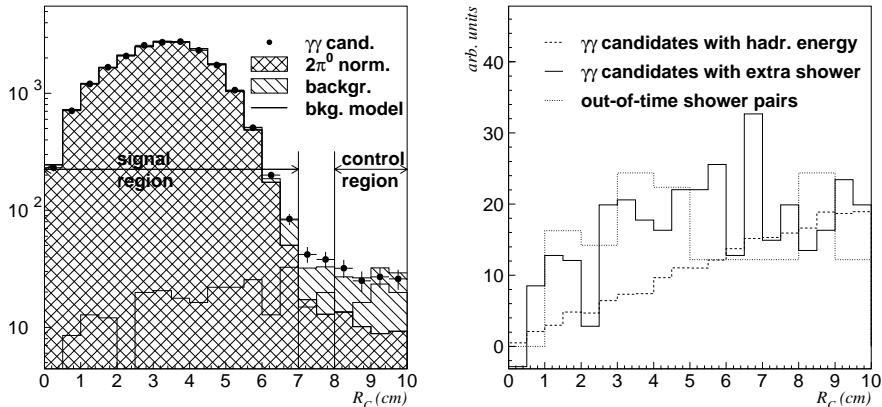

Figure 1: *Left:* Example of background subtraction in the near-target $\gamma\gamma$ sample using as a model $\gamma\gamma$ candidates with an extra shower. *Right:* Comparison of the centre-of-energy distributions of background models in the near-target data.
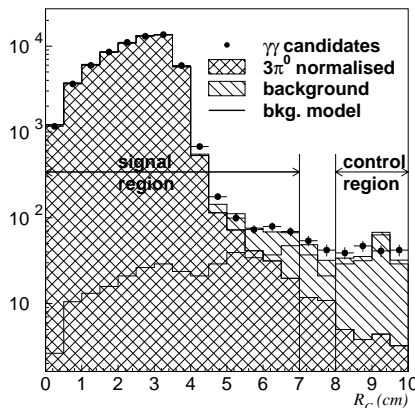

Figure 2: Background subtraction in the far-target $\gamma\gamma$ sample.

In order to subtract the $K_S \rightarrow \pi^0\pi^0$ background a sample of 1.2×10^9 decays was generated by Monte Carlo. The Monte Carlo sample was normalised using fully reconstructed $K_S \rightarrow \pi^0\pi^0$ events and checked by comparing it to the data in the 10 m following the decay region where $K_S \rightarrow \pi^0\pi^0$ background largely dominates the $\gamma\gamma$ sample (Fig. 3). The estimated background amounts to $(2.1 \pm 0.4)\%$ of the $K_S \rightarrow \gamma\gamma$ sample and populates mainly the last metre of the decay region. The uncertainty reflects a discrepancy between data and Monte Carlo in the simulation of overlapping showers.

The contribution of $K^0 \rightarrow ee\gamma$ decays to the $\gamma\gamma$ sample was estimated using Monte Carlo to be 0.4%. In the same way, the numbers of accepted $\pi^0\pi^0$ (0.9%) and $\pi^0\pi^0\pi^0$

(1.1%) decays with a subsequent $\pi^0 \to ee\gamma$ decay with respect to pure photon final states were estimated. The overall correction to the $BR(K_S \to \gamma\gamma)$ due to accepted Dalitz decays amounts to $(1.5 \pm 0.3)\%$, where the uncertainty is due to the simulation of overlapping showers.
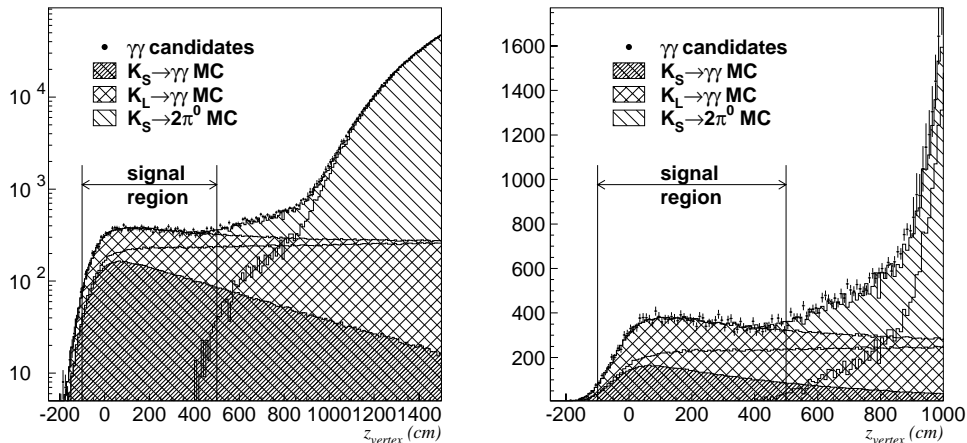

Figure 3: The z_{vertex} distribution of the near-target $\gamma\gamma$ sample with logarithmic (left) and linear (right) scales compared to Monte Carlo samples of $K_S \to \gamma\gamma$, $K_L \to \gamma\gamma$ and $K_S \to \pi^0\pi^0$ background, normalised to the flux and using the measured values of $\frac{\Gamma(K_L \to \gamma\gamma)}{\Gamma(K_L \to \pi^0\pi^0\pi^0)}$ and $BR(K_S \to \gamma\gamma)$. The shapes of the distributions before summing are also indicated.

6   Results

Binned maximum likelihood fits have been used to measure the $\frac{\Gamma(K_L \to \gamma\gamma)}{\Gamma(K_L \to \pi^0\pi^0\pi^0)}$ ratio and the $K_S \to \gamma\gamma$ branching ratio in 10 kaon energy and 6 longitudinal vertex position bins. Acceptances were calculated using Monte Carlo with detector simulation based on GEANT [11] where the LKr calorimeter response was simulated using a pregenerated shower library.

The ratio of $K_L \to \gamma\gamma$ and $K_L \to \pi^0\pi^0\pi^0$ decay rates, calculated from far-target samples and corrected for acceptance and for hadronic background as described in the previous section, is

$$\frac{\Gamma(K_L \to \gamma\gamma)}{\Gamma(K_L \to \pi^0\pi^0\pi^0)} = (2.81 \pm 0.01_{stat} \pm 0.02_{syst}) \times 10^{-3} \tag{5}$$

where the systematic uncertainty accounts for the uncertainties in the background subtraction and simulation of the calorimeter response in the acceptance calculation. The latter were checked by varying selection cuts, especially the shower-width cut in the $\gamma\gamma$ sample and the χ^2 cut in the $\pi^0\pi^0\pi^0$ sample, which are specific to each of these decay channels. In addition it was checked that the result is insensitive to various parameters, e.g. longitudinal vertex position and kaon energy.

The number of $K_L \to \gamma\gamma$ events in the near-target $\gamma\gamma$ sample is given by

$$N_{\gamma\gamma}^{near} = R_A \frac{N_{K_L \to \gamma\gamma}^{far}}{N_{K_L \to \pi^0\pi^0\pi^0}^{far}} N_{K_L \to \pi^0\pi^0\pi^0}^{near} \tag{6}$$

6

Hadronic background and accidentals	-2.1 ± 0.7 %
Background from $K_S \to \pi^0\pi^0$	-2.1 ± 0.4 %
Had. background in far-target beam	0.9 ± 0.4 %
Dalitz decay correction	1.5 ± 0.3 %
Acceptance uncertainty systematic	± 0.3 %
Acceptance uncertainty statistical	± 0.6 %
Trigger efficiency	± 0.1 %
Total	-1.8 ± 1.2 %
Statistical uncertainty data	± 2.0 %
BR($K_S \to \pi^0\pi^0$)	± 0.9 %

Table 1: Summary of all corrections and uncertainties in the BR($K_S \to \gamma\gamma$) measurement.

where N are the background corrected numbers of events from the near and far-target runs. R_A is a double ratio of acceptances

$$R_A = \frac{A_{K_L \to \gamma\gamma}^{near}}{A_{K_L \to \pi^0\pi^0\pi^0}^{near}} / \frac{A_{K_L \to \gamma\gamma}^{far}}{A_{K_L \to \pi^0\pi^0\pi^0}^{far}} \qquad (7)$$

which is close to unity (~ 1.05) because the same decay region was used for the far and near-target samples. For this reason only the background subtraction uncertainty in (5) enters the calculation of BR($K_S \to \gamma\gamma$), while the acceptance calculation uncertainty cancels between near and far-target samples.

The summary of all corrections and uncertainties in the BR($K_S \to \gamma\gamma$) calculation is given in Table 1. The acceptance uncertainty reflects the level of knowledge of non-Gaussian tails in the energy reconstruction accounted for in the acceptance calculation.

From 19819 $\gamma\gamma$ candidates, 7461 ± 172 have been estimated to be $K_S \to \gamma\gamma$ decays, giving a ratio of decay rates

$$\frac{\Gamma(K_S \to \gamma\gamma)}{\Gamma(K_S \to \pi^0\pi^0)} = (8.84 \pm 0.18_{stat} \pm 0.10_{syst}) \times 10^{-6} \qquad (8)$$

Using BR($K_S \to \pi^0\pi^0$) taken from [12] one obtains

$$BR(K_S \to \gamma\gamma) = (2.78 \pm 0.06_{stat} \pm 0.03_{syst} \pm 0.02_{ext}) \times 10^{-6} \qquad (9)$$
$$= (2.78 \pm 0.07) \times 10^{-6} \qquad (10)$$

where the external uncertainty is that quoted in Table 1 for the $K_S \to \pi^0\pi^0$ branching ratio. Systematic checks have confirmed that the result is stable with respect to longitudinal vertex position, kaon energy, run period and other parameters.

This result is in agreement with previous measurements, but has much better precision. It is the first measurement of $BR(K_S \to \gamma\gamma)$ to show significant difference with respect to the $O(p^4)$ calculations of χPT and indicates that higher order corrections increase the decay rate by about 30%.

ACKNOWLEDGEMENT

References

[1] G. D'Ambrosio and D. Espriu, Phys. Lett. B **175** (1986) 237.
J.L. Goity, Z. Phys. C **34** (1987) 341.
F. Buccella, G. D'Ambrosio and M. Miragliuolo, Il Nuovo Cimento A **104** (1991) 777.
J. Kambor and B.R. Holstein, Phys. Rev. D **49** (1994) 2346.

[2] Z.E.S. Uy, Phys. Rev. D **3** (1971), p. 234, and references therein.

[3] E. Ma and A. Pramudita, Phys. Rev. D **24** (1984) 2476.
J.F. Donoghue, B.R. Holstein and Y-C.R. Lin, Nucl. Phys. B **277** (1986) 651.

[4] G.D. Barr *et al.*, Phys. Lett. B **351** (1995) 579.

[5] A. Lai *et al.*, Phys. Lett. B **493** (2000) 29.

[6] N. Doble *et al.*, Nucl. Instr. Meth. B **119** (1996) 181.

[7] A. Lai *et al.*, Phys. Lett. B **533** (2002) 196.

[8] A. Lai *et al.*, Eur. Phys. J. C **22** (2001) 231.

[9] G. Unal for NA48 collaboration, 9th International Conference on Calorimetry, October 2000, Annecy, France, hep-ex/0012011.

[10] G. Barr *et al.*, Nucl. Instr. Meth. A **485** (2002) 676.

[11] GEANT Description and Simulation Tool, CERN Program Library Long Write-up W5013 (1994).

[12] Part. Data Group, Eur. Phys. J. C **15** (2000), 512.